Evaluation of lateral and axial resolution of pixel-based beamformers in photoacoustic tomography using a linear US probe.

Irene Pi-Martín, Alejandro Cebrecos, Juan J. García-Garrigós, Noé Jiménez, Francisco Camarena
Instituto de Instrumentación para Imagen Molecular (i3M)
Consejo Superior de Investigaciones Científicas (CSIC), Universitat Politècnica de València (UPV)
Valencia, Spain
irpimar@upv.es

2022 IEEE International Ultrasonics Symposium (IUS) | 978-1-6654-6657-8/22/$31.00 ©2022 IEEE | DOI: 10.1109/IUS54386.2022.9958843

***Abstract*—Many photoacoustic tomography (PAT) systems have been developed using conventional linear ultrasound probes with reduced angular spectra, which limits the resolution of tomographic reconstructions. These limitations are partially compensated by employing advanced reconstruction algorithms that take advantage of the intrinsic characteristics of the photoacoustic signals. The aim of this work is to theoretically, numerically and empirically characterise the lateral and axial resolution using two nearby point objects that are separated until they can be distinguished as two independent sources in the reconstructed image. It is also intended to study the effect of the main limitations of linear probes (geometry, frequency response and angular spectrum) on the spatial resolution. The results of this study shed light on the suitability of using each type of algorithm depending on the limiting conditions of the probe used and the imaging objective.**

***Index Terms*—photoacoustics, tomography, resolution, advanced algorithms**

I. Introduction

Photoacoustic (PA) imaging techniques use the ability of some materials (chromophores) to emit sound after being excited by pulsed light [1]. After laser excitation, the tissues undergo thermoelastic expansion and convert the optical energy into acoustic energy by emitting an ultrasonic wave. It propagates omnidirectionally and can be recorded with a typical ultrasonic (US) acquisition system to conform medical images [2]. This technique allows to differentiate the chromophores of the tissue, since each chromophore has a characteristic absorption spectrum, which makes it a promising medical imaging technique, with molecular contrast, better resolution than pure ultrasound imaging, and greater tissue penetration than optical techniques [3].

The three main photoacoustic imaging modalities are optical (OrPAM) and acoustic (ArPAM) resolution microscopy and tomography (PAT) [3]. This work focuses on photoacoustic tomography, which consists of pulsed illumination of the entire tissue to be imaged and the reception of the acoustic waves generated after excitation in the tissue. Both PAT and ArPAM are acoustic resolution techniques [3].

Spatial resolution is one of the most important parameters in photoacoustic reconstruction. Since biological tissues are not acoustically homogeneous, medical images obtained using this technique are usually foggy, although in some cases the blurring can be corrected [4]. Furthermore, since the photoacoustic pulse is omnidirectional and has fast rise times, it has content at very high frequencies and is detectable in all directions, so that the frequency response and aperture of the piezoelectric will also limit the resolution of future reconstructions [5]. The theoretical lateral and axial resolution of an acoustic resolution photoacoustic imaging system are defined by

$$R_L = 0.71 \cdot \frac{c}{\mathrm{NA} \cdot \mathrm{f_c}} \tag{1}$$

$$R_A = 0.88 \cdot \frac{c}{\Delta f} \tag{2}$$

where R_L and R_A are the lateral and axial resolution respectively, c is the speed of sound in the medium, NA is the numerical aperture, f_c is the centre frequency and Δf is the bandwidth of the probe [5].

Conventional ultrasonic linear phased arrays can be used in PAT, however, their limited angular spectra reduces the quality of the obtained images since some of the diverging laser-generated acoustic waves cannot be captured [6], therefore, reconstruction artefacts occur. To mitigate them, advanced time-based, frequency-based or pixel-based algorithms can be used [7].

The resolution of such systems has traditionally been defined by using point sources and measuring the full width at half maximum (FWHM) on their point spread function (PSF) [4]. Some studies have defined the resolution of their system as the difference between the FWHM and the actual object size based on the Rayleigh criterion [8].

However, a more practical definition of spatial resolution, commonly used in imaging systems, is the ability to differentiate between two objects in close proximity. Therefore, the resolution of a photoacoustic imaging system can be also defined as the minimum separation distance of two point sources at which it is possible to identify each source as an independent emitter. Following this idea, in [9] the resolution of microscopy systems is measured using two absorbers at

Authorized licensed use limited to: UNIVERSIDAD POLITECNICA DE VALENCIA. Downloaded on December 08,2022 at 10:20:26 UTC from IEEE Xplore. Restrictions apply.

different distances and determining at what point they are visually differentiated [9].

In this work, the PAT resolution has been evaluated with a quantitative criterion using images of very small objects of known size, on which the PSF can be applied. The main objective of this study is to determine numerically and empirically the lateral and axial resolution applying this practical criterion, as compared to their theoretical value, on PAT systems based on linear probes. The effect on the spatial resolution is then gauged, regarding geometry, frequency response and angular spectrum, for different advanced pixel-based beamformers.

II. Methods

To determine the resolution of the system, two point-like absorbers initially overlapped, are separated, on the horizontal and on the vertical axis relative to the probe, until it is possible to identify them as two independent sources in the reconstructed image. This study has been carried out both numerically and experimentally.

A. Numerical simulations

A set of 3D numerical simulations has been done with the k-Wave MATLAB toolbox. Two 0.1 mm diameter cylindrical sources and a linear probe have been simulated with the geometry and number of elements of the Verasonics L11-5v probe. In order to study the effect of the probe aperture and its frequency response, these parameters have been introduced into simulations.

The next simulated conditions, 2 and 3, correspond to the characteristics of condition 1 but adding limitations with a frequency response centred at 7.6 MHz with a 77 % bandwidth and the array element directivity limited to 0.5 rad respectively.

Finally, in simulation condition 4, it has been sought the most realistic scenario for the L11-5v probe in order to be able to compare the simulated data with the experiments and to validate the numerical results. In consequence, the geometric limitations (Sim. Cond. 1), the frequency response (Sim. Cond. 2) and the directivity (Sim. Cond. 3) have been considered in this case.

B. Experiments

Black nylon wires of 0.1 mm diameter fixed at the desired distances using a 3D-printed wire holder were excited with an Optical Parametric Oscillator (OPO) laser tuned at 532 nm, with beam cross-section diameter of 15 mm, 10 Hz pulse repetition rate and a pulse energy of 30 mJ. The PA signals were recorded by the Verasonics Vantage 256^{TM} ultrasound system with the L11-5v linear phased-array.

C. Image reconstruction

Four pixel-based beamforming algorithms have been implemented: Delay And Sum (DAS) [10], Delay Multiply and Sum (DMAS) [11], [12], Minimum-Variance (MV) [13] and MV-DMAS [14]; and, then, have been evaluated experimentally and numerically. DAS is the basic ultrasonic beamformer algorithm although some improvements have emerged seeking to take advantage of the spatial coherence of photoacoustic signals, which led to more complex algorithms such as the DMAS, or even to adaptive algorithms such as MV.

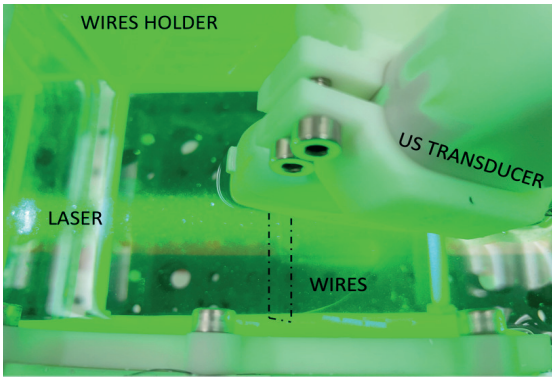


Fig. 1. Experimental set-up.

D. Data post-processing

In order to establish the empirical resolution of the system, a parameter called the Peak-to-Valley difference has been defined, which consists of calculating the difference between the signal level of the sources and the valley between them in the reconstructed image. The following criterion has been applied: when the difference is less than 3 dB, it is considered that the two sources cannot be resolved as independent entities; if it is between 3 and 6 dB, it is determined that both sources can be distinguished, although they are not yet resolved; and, if the distance between the sources and the valley is greater than 6 dB, it is considered that both sources have been fully resolved.

III. Results

The main results of this study are presented below. They can be classified into four blocks or stages: image reconstruction, profiles, evolution of the Peak-to-Valley parameter as a function of the separation between sources and, finally, the characterisation of the system resolution. To illustrate the first two blocks, the particular case where the sources are 0.5 mm apart has been selected.

A. Image reconstructions

Fig. 2 shows the reconstructed images using the simulation data of condition 4 (labeled as Sim.) and the experimental data (labeled as Exp.). From the reconstructed images, it can be seen that the simulations of the more realistic condition are apparently in good agreement with the experiments. Furthermore, it is observed that, as the complexity of the algorithms increases, the Signal-to-Noise ratio (SNR) of the image improves since, with the same dynamic range, the secondary lobes are much more prominent in DAS than in MV-DMAS. Besides, for the source separation distance shown in this figure, it can be seen that the algorithm used is critical in order to be able to resolve the sources. Indeed, for the specific case of the figure, both sources can be resolved by reconstructing with MV-DMAS but not with DAS.

Authorized licensed use limited to: UNIVERSIDAD POLITECNICA DE VALENCIA. Downloaded on December 08,2022 at 10:20:26 UTC from IEEE Xplore. Restrictions apply.

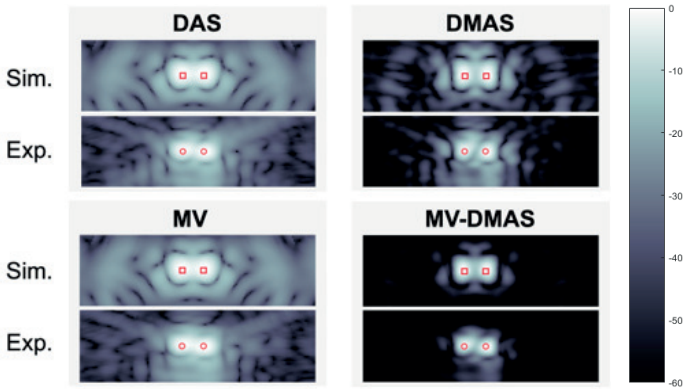


Fig. 2. Reconstruction of simulated and experimental images using the four pixel-based algorithms displayed with a dynamic range of 60 dB. The actual size of the sources, which have a cross-section of 0.1 mm, is shown in red.

B. Lateral and axial profiles

In order to quantitatively assess the above-mentioned aspects of the reconstructions, the lateral and axial profiles have been used to obtain their corresponding resolution values. Fig. 3 shows the profiles of the simulation under realistic conditions (continuous black line) and the experimental profiles (dashed blue line). The agreement between simulation and experiments is thus used to validate the numerical study.

Moreover, it can be seen how, for the same data set, empirical or simulated, when the DAS still not distinguish the two emitters as independent entities, some algorithms allow the sources to be resolved as independent emitters. For example, in MV-DMAS it is evident that the difference between the peaks, corresponding to adjacent sources, and the valley between them is greater than 6 dB.

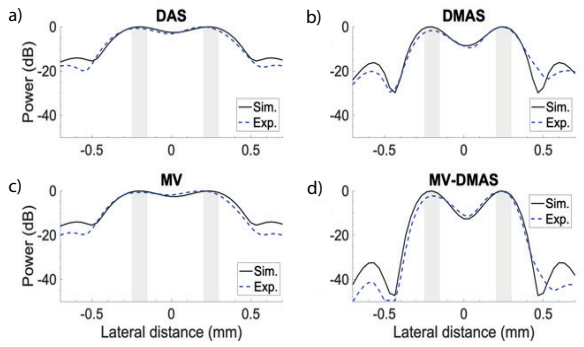


Fig. 3. Reconstruction profiles of simulated and experimental images using the four pixel-based algorithms. The grey columns represent the actual sources.

C. Peak-to-Valley parameter (PV)

If the difference between the peaks and the valley (PV) for each of the distances studied is calculated, the resolution for each of the simulated conditions and for the experiments carried out can be determined based on the resolution criterion of a PV distance greater than 6 dB. The evolution of this parameter as the distance between sources in the lateral and axial axis increases is shown in Fig. 4 and Fig. 5 respectively.

In these graphs, three situations can be differentiated: green area shows where the sources are resolved as independent entities for PV difference of more than 6 dB, yellow area shows the distances where they cannot be resolved but can be distinguished, between 3 and 6 dB PV, and red area shows the distances where they could neither be resolved nor distinguished, below 3 dB PV.

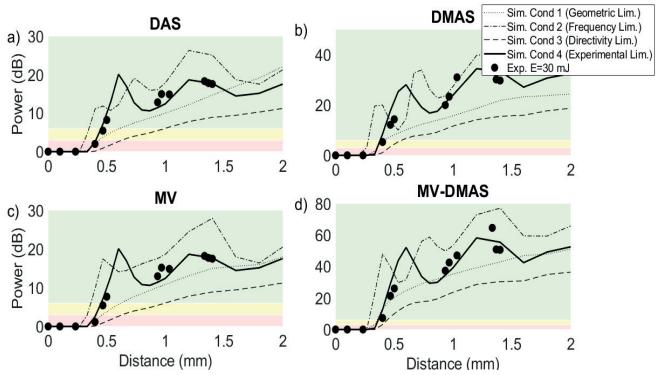


Fig. 4. Evolution of peak-to-valley distance parameter as the distance between sources on the lateral axis increases.

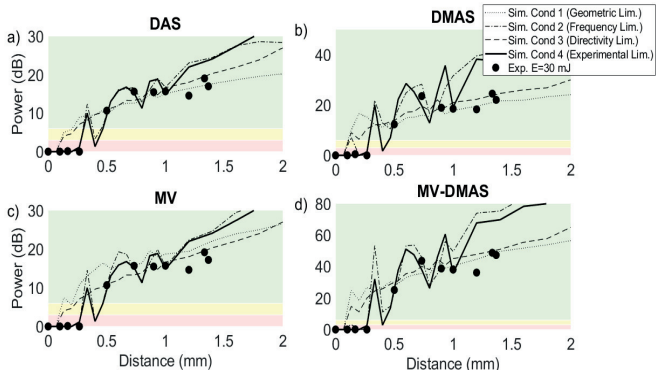


Fig. 5. Evolution of peak-to-valley distance parameter as the distance between sources on the axial axis increases.

From this results it is observed that MV beamforming allows to stay close to the theoretical axial resolution, even if the frequency response is limited (Sim. Cond. 2). DMAS stands out for its ability facing aperture limitations (Sim. Cond. 3), which mainly affect lateral resolution. Eventually, MV-DMAS is the one that offers the best resolution in all the conditions studied, both numerical and experimental. Note that the results of the simulations are experimentally validated by the visible agreement between the results of simulated Cond. 4 and the experiments.

D. System resolution

The lateral and axial resolutions are respectively obtained experimentaly and numerically under realistic simulation conditions (Sim. Cond. 4), so that the resolution of the system

Authorized licensed use limited to: UNIVERSIDAD POLITECNICA DE VALENCIA. Downloaded on December 08,2022 at 10:20:26 UTC from IEEE Xplore. Restrictions apply.

with the L11-5v linear probe is determined for the proposed beamformers. The resolution of the system calculated numerically and empirically are shown in Tables I and II.

TABLE I
LATERAL RESOLUTION

R_L	***DAS***	***DMAS***	***MV***	***MV-DMAS***
Experiments (mm)	0.473	0.406	0.474	0.369
Numerics (mm)	0.451	0.379	0.448	0.362

* Numerical results on Sim. Cond. 4.

TABLE II
AXIAL RESOLUTION

R_A	***DAS***	***DMAS***	***MV***	***MV-DMAS***
Experiments (mm)	0.303	0.284	0.302	0.275
Numerics (mm)	0.395	0.380	0.396	0.322

* Numerical results on Sim. Cond. 4.

On the other hand, using equations (1) and (2), the theoretical lateral and axial resolutions have been calculated, being R_L = 0.21 mm and R_A = 0.23 mm, respectively. The theoretical results are lower than the numerical and experimental ones, which may indicate that the theory is not taking into account neither the spacing between probe piezoelectric elements nor the width of each element.

IV. CONCLUSIONS

These results show that the applied beamformers become especially relevant when chromophore separation is near to the resolution limit. MV is in good agreement with the theoretical axial resolution even if the frequency response is limited, while DMAS stands out for its ability facing aperture limitations, which mainly affects lateral resolution. Finally, it has been shown that MV-DMAS is the one that offers the best resolution for all the conditions studied, both numerical and experimental. The results of the simulations has been experimentally validated, obtaining an excellent agreement between experiments and the most realistic simulation of the probe. The obtained results helps in the choice of the most suitable beamformer when limitations of geometry, frequency response and directivity are considered for linear probe based tomography systems.

ACKNOWLEDGMENT

We thank financial support from Generalitat Valenciana through the programs Prometeo CIPROM/2021/003 and Equipamiento e Infraestructuras FEDER 2021-22 IDIFEDER/2021/004, and Agència Valenciana de la Innovació INNVA2/2022/11.

REFERENCES

[1] A. Graham Bell, "On the Production and Reproduction of Sound by Light," Proc. Am. Assoc. Adv. Sci., vol. 29, pp. 115–136, 1881.

[2] R. A. Kruger, P. Liu, Y. "Richard" Fang, and C. R. Appledorn, "Photoacoustic ultrasound (PAUS)—Reconstruction tomography," Med Phys, vol. 22, pp. 1605–1609, 1995.

[3] P. Beard, "Biomedical photoacoustic imaging," Interface Focus, vol. 1, no. 4. Royal Society, pp. 602–631, 2011. doi: 10.1098/rsfs.2011.0028.

[4] M. Xu and L. v. Wang, "Analytic explanation of spatial resolution related to bandwidth and detector aperture size in thermoacoustic or photoacoustic reconstruction," Phys Rev E Stat Phys Plasmas Fluids Relat Interdiscip Topics, vol. 67, no. 5, p. 15, 2003, doi: 10.1103/PhysRevE.67.056605.

[5] J. Yao and L. v. Wang, "Photoacoustic microscopy," Laser Photon Rev, vol. 7, no. 5, pp. 758–778, Sep. 2013, doi: 10.1002/lpor.201200060.

[6] Y. Xu, L. v. Wang, G. Ambartsoumian, and P. Kuchment, "Reconstructions in limited-view thermoacoustic tomography," Med Phys, vol. 31, no. 4, pp. 724–733, 2004, doi: 10.1118/1.1644531.

[7] C. Tian, M. Pei, K. Shen, S. Liu, Z. Hu, and T. Feng, "Impact of System Factors on the Performance of Photoacoustic Tomography Scanners," Phys Rev Appl, vol. 13, no. 1, Jan. 2020, doi: 10.1103/PhysRevApplied.13.014001.

[8] L. Zeng, G. Liu, D. Yang, and X. Ji, "3D-visual laser-diode-based photoacoustic imaging," Opt Express, vol. 20(2), pp. 1237–1246, 2012.

[9] L. Zeng, G. Liu, D. Yang, and X. Ji, "Portable optical-resolution photoacoustic microscopy with a pulsed laser diode excitation," Appl Phys Lett, vol. 102, no. 5, Feb. 2013, doi: 10.1063/1.4791566.

[10] V. Perrot, M. Polichetti, F. Varray, and D. Garcia, "So you think you can DAS? A viewpoint on delay-and-sum beamforming," Ultrasonics, vol. 111, Mar. 2021, doi: 10.1016/j.ultras.2020.106309.

[11] G. Matrone, A. S. Savoia, G. Caliano, and G. Magenes, "The delay multiply and sum beamforming algorithm in ultrasound B-mode medical imaging," IEEE Trans Med Imaging, vol. 34, no. 4, pp. 940–949, Apr. 2015, doi: 10.1109/TMI.2014.2371235.

[12] T. Kirchner, F. Sattler, J. Gröhl, and L. Maier-Hein, "Signed real-time delay multiply and sum beamforming for multispectral photoacoustic imaging," J Imaging, vol. 4, no. 10, Oct. 2018, doi: 10.3390/jimaging4100121.

[13] B. M. Asl and A. Mahloojifar, "Minimum variance beamforming combined with adaptive coherence weighting applied to medical ultrasound imaging," IEEE Trans Ultrason Ferroelectr Freq Control, vol. 56, no. 9, pp. 1923–1931, Sep. 2009, doi: 10.1109/TUFFC.2009.1268.

[14] M. Mozaffarzadeh, A. Mahloojifar, M. Orooji, K. Kratkiewicz, S. Adabi, and M. Nasiriavanaki, "Linear-array photoacoustic imaging using minimum variance-based delay multiply and sum adaptive beamforming algorithm," J Biomed Opt, 2018, doi: 10.1117/1.JBO.23.2.026002.

Authorized licensed use limited to: UNIVERSIDAD POLITECNICA DE VALENCIA. Downloaded on December 08,2022 at 10:20:26 UTC from IEEE Xplore. Restrictions apply.